Hindawi
Advances in Materials Science and Engineering
Volume 2019, Article ID 1340934, 14 pages
https://doi.org/10.1155/2019/1340934

Research Article

Mechanical Properties and Failure Modes of Rock Specimens with Specific Joint Geometries in Triaxial Unloading Compressive Test

Guoyong Duan,[1,2,3] **Jianlin Li**,[1,2,3] **Jingyu Zhang**,[3] **Eleyas Assefa**,[4] **and Xushu Sun**[3]

[1]*Key Laboratory of Ministry of Education for Geomechanics and Embankment Engineering, Hohai University, Nanjing 210098, China*
[2]*Jiangsu Research Center for Geotechnical Engineering Technology, Hohai University, Nanjing 210098, China*
[3]*Key Laboratory of Geological Hazards on Three Gorges Reservoir Area, Ministry of Education, China Three Gorges University, 8 Daxue Road, Yichang 443002, China*
[4]*College of Architecture and Civil Engineering, Addis Ababa Science and Technology University, Addis Ababa, Ethiopia*

Correspondence should be addressed to Xushu Sun; sunxs@ctgu.edu.cn

Received 21 August 2018; Revised 26 January 2019; Accepted 14 February 2019; Published 25 March 2019

Academic Editor: Jun Liu

The effects of disconnected joints on the mechanical characteristics of rock masses are interesting and challenging aspects of rock mechanics. The prime objective of this study is to investigate the effect of joint orientations and joint connectivity rates on the strength, deformation, and failure mechanisms of rock specimens under unloading condition. To establish the relationships between different factors (confining pressure, joint orientation, and joint connectivity) and failure mechanisms, a series of triaxial unloading tests were performed. The results showed that the joint orientation had a more considerable effect than the joint connectivity on the strength and deformation of the specimens. Generally, three different types of failures were observed (i.e., shear, mixed, and split). Finally, Griffith's theory was utilized to analyze the maximum tensile stress around the crack. The findings of this paper can also be used for practical engineering problems.

1. Introduction

Understanding the mechanical behavior of jointed rock is very important for stratum stability in gas and oil engineering [1]. The stress release and redistribution around the excavation surface generally results in deformation of rock mass together with expansion and extension of existed discontinuities and development of macroscopic fractures. The discontinuities (such as joints, fissures, faults, cleavages, and bedding planes) can significantly affect the mechanical behavior of jointed rock mass [2, 3].

Several attempts [4–6] have been made in the past to investigate the influence of fractures on the macroscopic behavior of the rock mass and to illustrate the crack propagation mechanisms.

Practically, it is too difficult to find a homogeneous rock with a single discontinuity. Therefore, researchers have used rock-like materials to investigate the effects of cracks on the mechanical properties of rock masses. Cao et al. [7] conducted a series of uniaxial compression tests on similar materials to simulate the effect of preexisting joints and fissures of rock. The variation of joint orientation draws the attention of researchers. Cracks easily initiated at the tips of discontinuity when the angles of inclination were 0°, 30°, and 60° under a series of uniaxial compression tests [8]. Bing et al. [9] performed the test on gypsum specimens containing a single discontinuity with length 10 mm–30 mm and different inclination angles 0°–90°. The resulting peak stresses were affected by both factors. Meanwhile, the discontinuity scale was studied as a critical factor by Zhang [10] through the acoustic emission monitoring system in the uniaxial compression test. Similar patterns of crack propagation were observed through numerical simulation. Meng and Liu [11] used RFPA software to simulate the relationship between a rock mass with one discontinuity and different confining pressures. According to their result, the crack was

extended vertically at low confining pressure and traced a horizontal trend at a high confining pressure.

Based on the above facts, the uniaxial compression test was predominantly used in the last decades. It has two advantages as shown below: (1) uniaxial loading equipment is conventional in the laboratory and convenient for multiscale specimens and (2) one can efficiently use high-speed cameras and acoustic emission monitoring instrument during the experiment. However, a uniaxial compression test is merely applicable to stimulate free face in mining and excavation. Underground rock mass with a three-dimensional stress state is another research topic in practice. The mechanical behavior of rock material under the biaxial and triaxial conditions is beneficial to explore the failure mechanism of rock engineering.

Sagong et al. [12] conducted the biaxial compression test on specimens with different orientations (30°, 45°, and 60°). They discovered that tensile crack initiation and propagation plays a dominant role at a small joint dip angle. In contrast, tensile cracks exhibit abrupt initiation and propagation under large joint angle. Chen et al. [13] conducted a series of conventional triaxial compression tests to scrutinize the prefailure damage characteristics. According to their study, the damage propagation rate varied distinctly before the reversal of the volumetric strain. Yang et al. [14] performed cyclic triaxial tests and categorized four stages based on Poisson's ratio and Young's modulus parameters. Erarslan [15] focused on micromechanical and microstructural dynamics to study subcritical crack propagation. Wang et al. [16] studied the effects of the joint dip angle by using distinct element-based numerical simulations. More cracks developed when the joint dip angles were small.

Although the influences of rock joints on the strength, deformation, and failure mechanism have been studied analytically, numerically, and experimentally, loading conditions are merely a glimpse of the problems in practice. This concept is discussed with a practical engineering problem below. As it is known, China Three Gorges Dam is the biggest hydropower project in the world. The reservoir is 185 meters deep, with a storage capacity of about 39.3×10^9 m^3. Due to its large storage capacity and cyclic fluctuation, the rock masses in the vicinity of the Three Gorges Reservoir area have been repeatedly subjected by loading and unloading process with respect to its geological age (Figure 1). As a result of similar large-scale project constructions and long-term operation in the high-stress region, the unloading effect on the rock mass became a frontier topic.

Laboratory investigations [17, 18] and numerical simulations [19] revealed the fact that the behavior of rock under unloading condition is different from that of loading condition. Li et al. [20] proposed a new micromacromethod to predict the shear strength of the brittle rock by relating crack propagation with the axial strain. The fractal values of sandstone samples were used to predict the failure precursors at low and high confining pressures and rock failure at low and high confining pressures, respectively [21]. The axial, circumferential, and volumetric deformations at stress level close to the peak stress result in a considerable volume expansion and a large deformation platform during the unloading process [22]. Stress relaxation behavior was studied under loading and unloading conditions [23]. They found that the rate of unloading is closely related to the stress relaxation behavior. In the stress relaxation test, the failure is due to tensile rheological cracks of smooth coalescence. However, the fracture in the traditional compression test is related to the wing cracks with abrupt coalescence. From the perspective of energy conversion, Li et al. [24] compared the released elastic strain energy with the absorbed energy in the triaxial unloading tests. The increased rate of energy dissipation widely varies between the triaxial loading and unloading conditions. New models were proposed for the brittle rocks by the researchers. Zhou et al. [19] presented a phase field model to study crack propagation, branching, and concentration of coalescence on twenty parallel flaws and multiple echelon flaws. Liu and Zhang [25] established a model considering the coeffect of macroscopic and mesoscopic flaws based on the Lemaitre strain equivalence.

Now the existing study on the crack damage of rock mechanics is often based on the uniaxial compression tests, which is well developed and understood. However, the study on flaw propagation under the unloading condition is not relatively enough since existing studies predominantly considered a single flaw parameter to analyze the anisotropic behavior of the rock mass with a consideration of the joint geometrical properties such as its length and dip angle. However, its mechanical theory was not studied very well. Hence, there is a lack of theoretical analysis of the test results.

Therefore, in this paper, the results of a series of conventional triaxial loading and unloading tests on a rock-like material containing a single flaw under variable confining pressures ranging between 0 and 10 MPa were theoretically analyzed and interpreted. Based on the crack damage modes, the coeffect of the joint angle and joint connectivity on the strength and deformation parameters was investigated. Then, the effects of the confining pressure on the propagation and joint type were analyzed. Finally, the damage characteristics of the specimens were analyzed using Griffith's strength theory in detail.

2. Testing Specimens (Sample Preparation)

Considering the discreteness and the difficulty in acquiring a natural rock together with disconnected joint, a cement mortar was prepared from a mix of ordinary Portland cement (OPC), sand, and water at the ratio of 1 : 1.73 : 0.4, respectively, by weight. The strength parameters of the cement mortar were similar to the weak weathering sandstone in China Three Gorges Reservoir Region. The parameter comparisons between sandstone and cement mortar are listed in Table 1. Due to the similarity-based parameters, the cement mortar is reasonably selected as a rock-like material.

Afterwards, the cement mortar was poured into a cylindrical plastic mold (i.e., 50 mm inner diameter by 105 mm height). A small size shaking table system was employed to eliminate the development of bubbles during sample preparation. As shown in Figure 2, symmetrical grooves were established on the surface of cylindrical molds to create

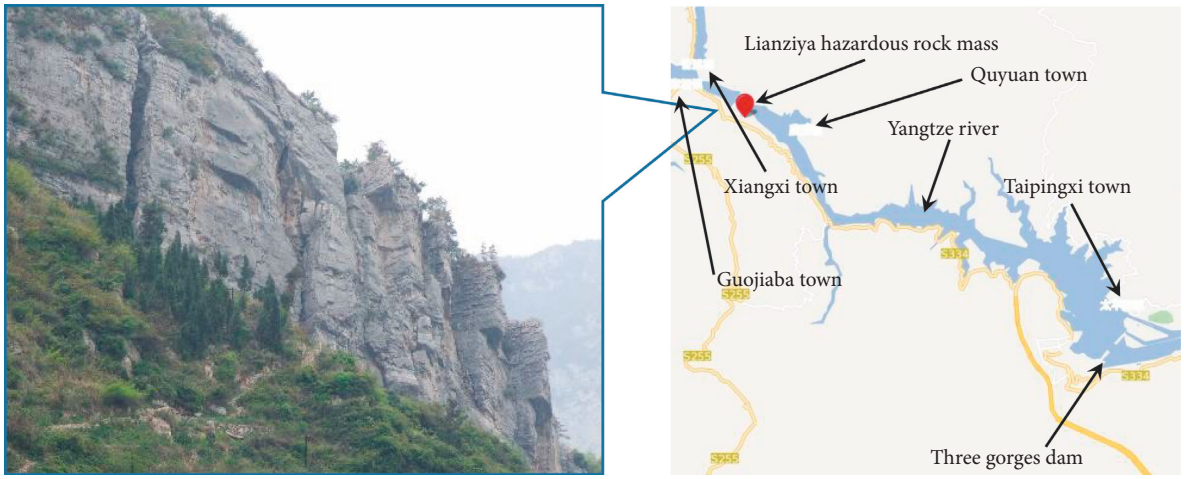

Figure 1: Lianziya hazardous rock mass in Three Gorges Reservoir area.

Table 1: The parameter comparisons between sandstone and cement mortar.

	Sandstone	Cement mortar
Cohesion (MPa)	16.2	10.7
Internal friction angle (°)	35	31.5
Uniaxial compression strength (MPa)	39.29	32.65
Elasticity modulus (GPa)	10.25	9.24
Poisson's ratio	0.40	0.38
Unit weight (kN/m^3)	22.0	20.6

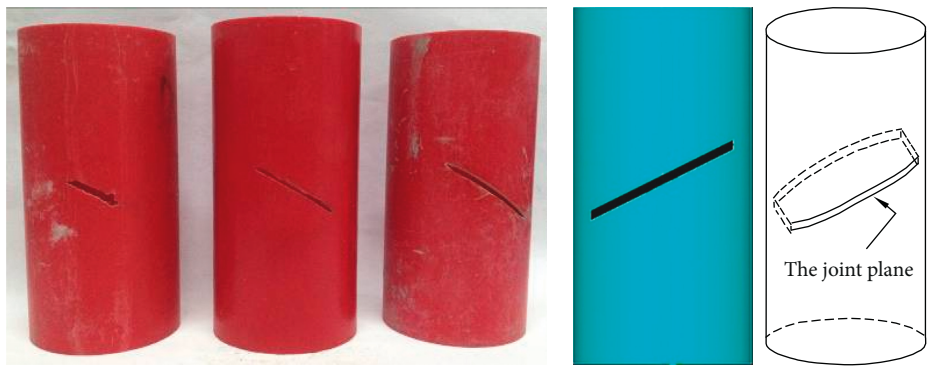

(a) (b)

Figure 2: Schematic diagram of specimens. (a) Cylindrical plastic molds used for sample preparation. (b) Joint location and joint connectivity rate.

joints with thin steel sheets. A release agent was presmeared inside the molds and the steel sheets to extrude the samples smoothly after the initial set time. Due to the presence and extraction of thin sheets, the joints were developed during solidification. Then the cement mortar samples were kept in a curing room (at 18°C room temperature, 99% relative humidity, and atmospheric pressure for 28 days). No fillers were employed inside the joint openings (all of the opening widths were less than 1 mm). To get flat surfaces, the tips of the specimens were trimmed off.

2.1. Joint Geometries Created to Observe the Influence of Joint Connectivity Rate. The first set of triaxial compression test was executed to investigate the effect of joint connectivity rate on the mechanical properties of the specimens with partially cut-through joints. Here, the angle of inclination was kept constant. It is defined as the ratio between the joint area and the joint location plane, across the specimen as shown in Figure 2. Meanwhile, k stands for joint connectivity rate, and three different values were considered (0.30, 0.45, and 0.60). However, all the other joint geometrical

parameters were kept constant. The joints were symmetrically located at the center of the specimen to minimize the conceivable effect of eccentricity.

2.2. Joint Geometries Created to Observe the Influence of Joint Orientation. The other set of triaxial compression test was performed to investigate the effect of joint orientation on the mechanical response of the specimens with partially cut-through joints. In this case, the joint connectivity rate was kept constant. The centroid of the joint was located at 50 mm distance from the tip of the specimen. Three different values were adopted as joint orientations (i.e., 30, 45, and 60°). The joint orientations were measured from the horizontal axis. Except the joint orientation, the other geometrical parameters were kept constant. Based on the Mohr–Coulomb failure criterion, the dip angle of the structural plane with respect to the intact failure surface is slightly larger than 45°. As a result, one can investigate the impact of joint orientation by altering the angles. Figure 3 shows the geometrical specifications used for preparing nine different specimens.

3. Description of Laboratory Test

In this testing program, a computerized triaxial compressive testing apparatus was used as shown in Figure 4.

This device (RMT-150C) was designed and manufactured by the Institute of Rock and Soil Mechanics (affiliated to the Chinese Academy of Sciences). It can simulate the loading and the unloading conditions and perform different types of tests (uniaxial test, direct shear test, Brazil disk split test, etc.).

The PCI-2 AE screening system was used to eliminate the specimens with defects.

4. Experimental Methodology

To investigate the mechanical properties of rock mass with disconnected joints, especially under loading and unloading conditions, five different values of confining pressures and different kinds of stress paths were adopted as listed in Table 1.

The adopted testing procedures for the cylindrical rock specimens are as follows:

(1) Initially, the "force-confining pressure" mode was selected, and a predefined axial force and confining pressures were applied on the specimens simultaneously, at the loading rate of 0.2 kN/s and 0.1 MPa/s, respectively. The axial load was increasing at the rate of 0.5 kN/s until failure occurred at a constant confining pressure. Then, the maximum triaxial compression strength was determined.

(2) The same type of specimen was chosen.

(3) The "force-confining pressure" mode was selected, and a predefined axial force and confining pressures were applied on the specimens simultaneously, at the loading rate of 0.2 kN/s and 0.1 MPa/s, respectively.

(4) After setting the confining pressure constant, the axial load was applied at the rate of 0.5 kN/s up to the 70% of the maximum triaxial compressive strength.

(5) Then the confining pressure was unloaded to failure at a rate of 0.01 MPa/s. The predefined loadings for the specimen with 30° joint orientation and 0.3 connectivity rates are shown in Table 2.

5. Testing Results and Discussion

As it was mentioned in Section 4, the testing programme was designed to analyze the effect of joint orientation and connectivity rate on the mechanical properties of rock specimens with partially cut-through joints. Their effects on the compressive strength and deformation characteristics are discussed below.

Brittle failure occurred frequently in the triaxial unloading tests. The process of unloading was conducted by decreasing the confining pressure. Hence, the percentage of reduction in the confining pressure was a key factor which affected the sample failure. During the unloading tests, all the parameters were recognized as equivalent variables which were different from the typical parameters.

Through the analysis of the deformation modulus of the specimens with different dip angles and connectivity ratios, the variation of different types of deformation modulus with unloading is shown in Figure 5. The deformation modulus is represented as E_{50}, and $\Delta\sigma_3$ is the reduction percentage of the confining pressure. The results show that the deformation modulus of specimens with different connectivity ratios is similar under the same confining pressure level. As a result, the deformation modulus is less sensitive to the change of joint connectivity. As the inclination angle increases, the average value of the deformation modulus enlarges. Therefore, the deformation modulus is more sensitive to the change of the inclination angle. When the confining pressure level varies, the deformation modulus of the same type of specimens fluctuates slightly. It can be concluded that the confining pressures ranging from 0 MPa to 10 MPa have a little effect on the deformation modulus. According to the variation of the deformation modulus, a large decrease in the amplitude arouses at the unloading percentages of 0~20% and 80%~100%. Especially, after the 80% reduction of confining pressure, the deformation modulus declined rapidly. However, when the unloading loss ranges from 20%–80%, the decreasing amplitude is stable relatively. Accelerated variation crops up at the early stage and the late stage of unloading. During the triaxial unloading process, the internal strain of the specimen is accumulated by the confining pressure constraint. When the confining pressure is declining, accumulated energy release initiates gradually. The internal stress and strain are adjusted while maintaining the residual bearing capacity. Accordingly, the middle stage of deformation modulus alteration is relatively flat. At the end of unloading process, the residual confining pressure is insufficient to restrain the energy inside the specimen and thereupon failure occurs. Hence, the development of unloading procedure can be divided into two stages in

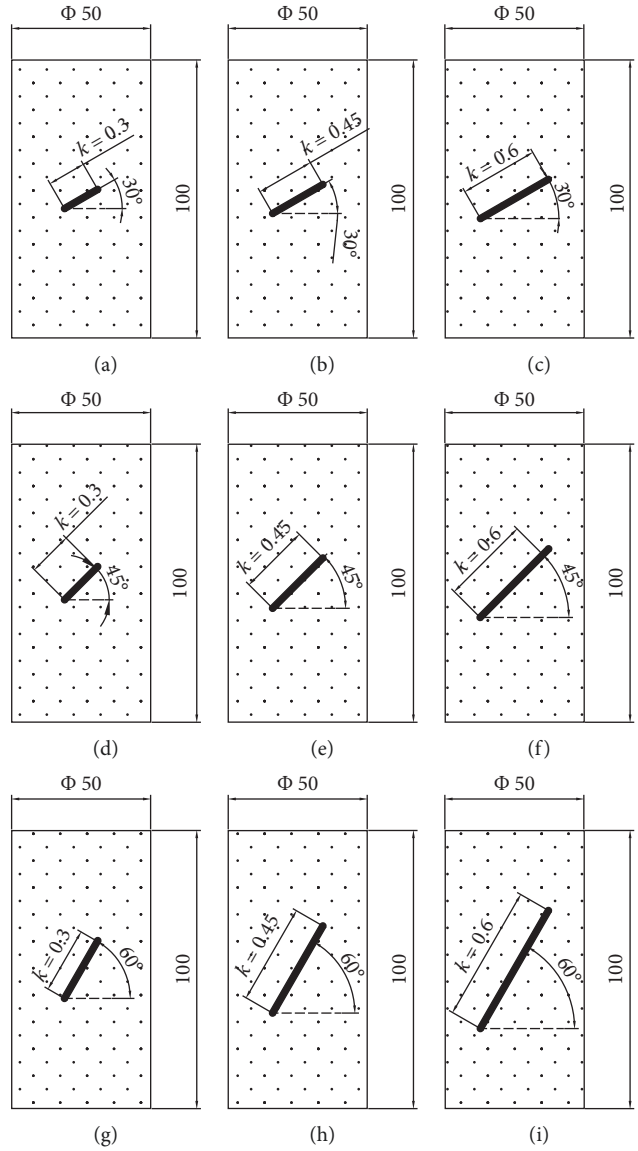

Figure 3: Geometrical specifications.

consonance with the decrease rate of deformation modulus. There are 0%~80% and 80%~100%, respectively.

6. Failure Modes

The failure modes of jointed samples were identified by the location and the size of cracks. The influence of joint parameters on the crack propagation was discussed. As shown in Figure 6, the failure modes were categorized into three groups.

(1) The shear failure occurred frequently under compression condition. It can be recognized by the shear plane. Ignoring stress concentrations on the boundaries of samples, the shear plane was relatively flat. This may be induced due to the conversion from defects to weak structural planes. Based on the assumption of sliding mostly occurs along the weak planes in rock mass, the joints are considered as weak structural planes. However, rupture did not transpired along the crack orientation completely during the test. In other words, the prefabricated cracks did not thoroughly affect the crack propagation in several cases (Figure 7(a)). The condition of a sample separated into two parts along the joints accounted for two third percentage. Joint geometries and the degree of coincidence between the joint and the rupture trajectory can be used to characterize the failure modes (Figure 3).

(2) Generally, splitting failure arises at lower confining pressures. The lateral deformation increases much more rapidly in the circumstances. And the splitting cracks were nearly parallel to the maximum principal stress of the sample. Meanwhile, the secondary cracks propagated from the crack tips during the

Figure 4: Triaxial compressive testing apparatus.

Table 2: Stress state for the triaxial compression and unloading compression.

Stress state	Minimum principal stress, σ_3 (MPa)	Maximum principal stress, σ_1 (MPa)	Remarks
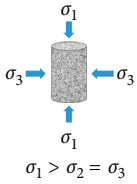	10	61.526	Triaxial compression
	8	55.468	Triaxial compression
	6	47.028	Triaxial compression
	4	37.239	Triaxial compression
	2	29.256	Triaxial compression
	10	43.106	Triaxial unloading compression
	8	38.677	Triaxial unloading compression
	6	32.110	Triaxial unloading compression
	4	25.502	Triaxial unloading compression
	2	20.060	Triaxial unloading compression

unloading tests. It is noteworthy that splitting failure occurs in the intact rock samples in the procedure of uniaxial compression. Nevertheless, similar phenomena were observed on the specimens with smaller joint angles and connectivity rates. In other words, the likelihood of splitting failure is high when the influence of joint is insignificant. Meanwhile, the probability of splitting failure is also dependent on the angle of the joint and the vertical axis of the sample. Based upon the results, samples with 30° joint orientation were more inclined to splitting failure.

(3) A mixed type of failure (tension and shear) was developed at higher joint orientation and medium joint connectivity rate. It is characterized by sliding of joints and development of tension cracks from the crack tip. Based on the rupture morphology, the precondition of mixed failure hinges on middle values of joint orientation and connectivity rate as shown in Figures 7(d)–7(f). Considering the tendency of shear along the joint plane, tension cracks developed by the reason of stress concentrations at the tips of the cracks. It is an important characteristic that reveals the dislocation of sample pieces before the ultimate failure. The two parallel tension fractures were normal to the original crack. In most cases, the secondary cracks were connected to the tips of joints where stress concentrations are inevitable. Therefore, the propagation of cracks can be determined by analyzing the geometries of joints and loading conditions.

6.1. Effect of Confining Pressure on the Failure of the Samples. In the triaxial test, the mechanical properties of rock specimens can be affected by the confining pressure definitely. The effect of unloading was remarkable when the confining pressures were 2 and 4 megapascals (based upon the analysis of 30 diagrams). As a result, the specimens exhibited different levels of damages at different confining pressures. During the unloading test, parts of the specimens were shattering when the confining pressure was lower, for example, 2 and 4 megapascals. In this case, the fragments

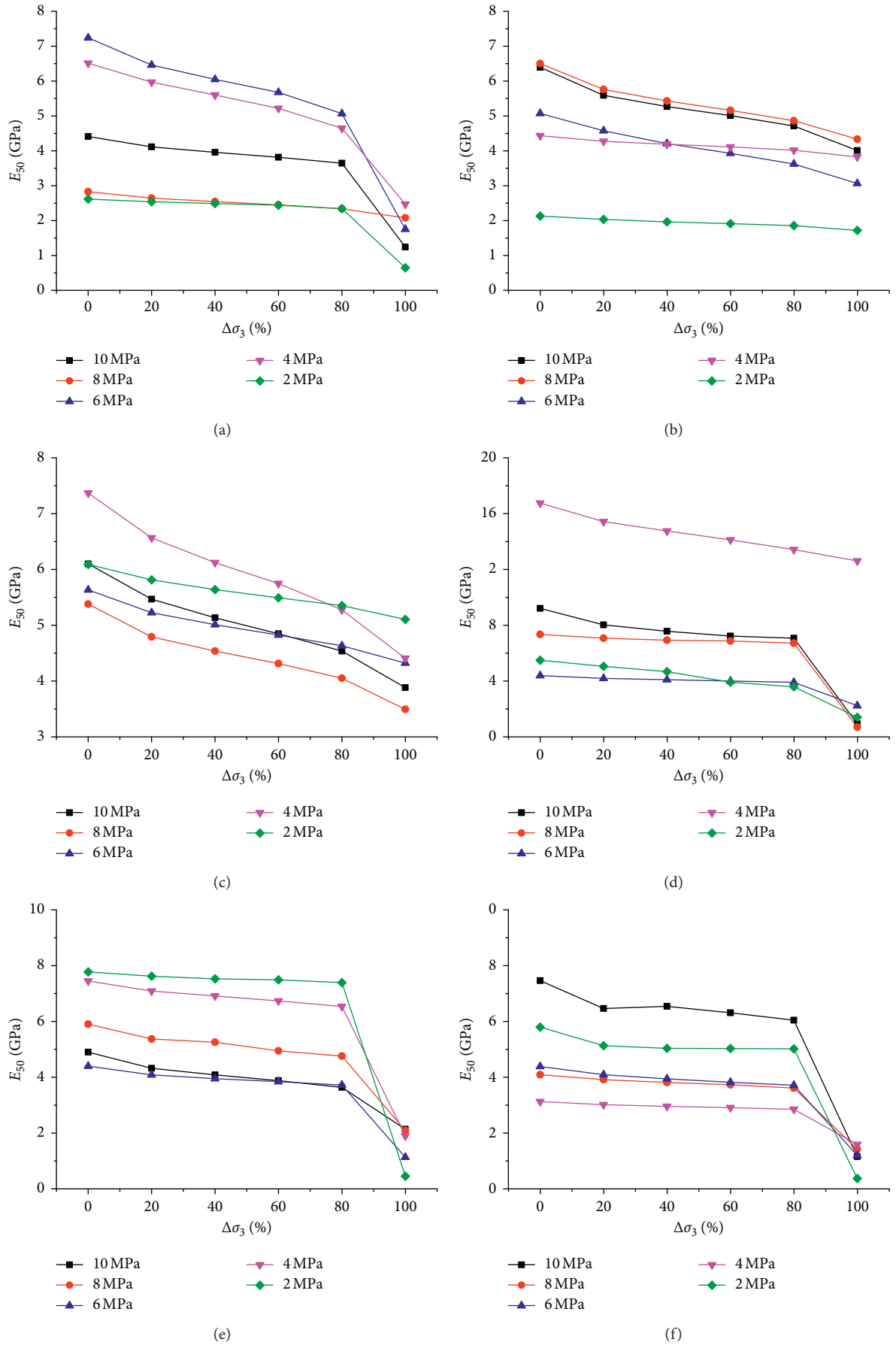

Figure 5: Continued.

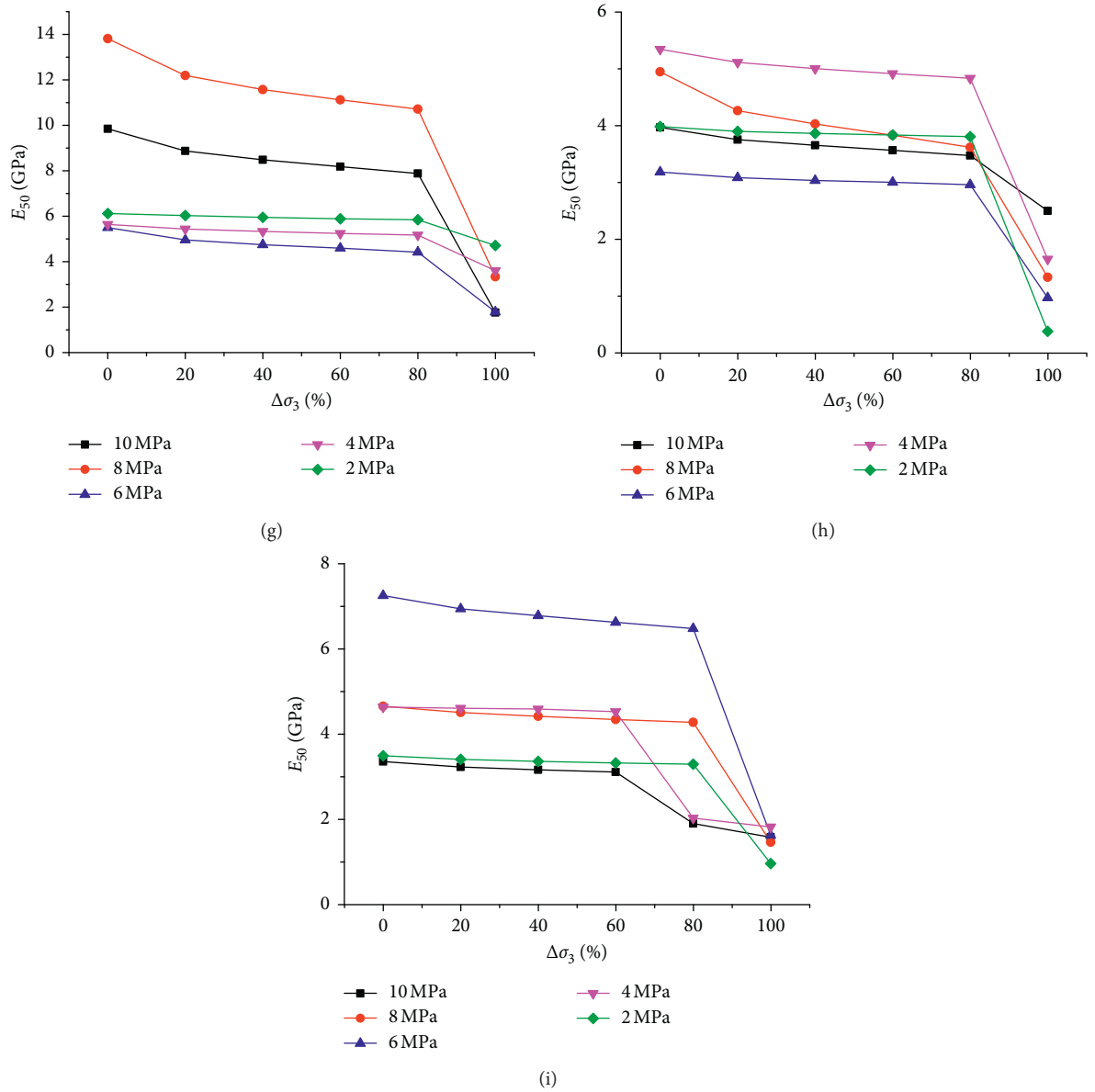

Figure 5: Relationship between deformation modulus and unloading percentage (joint orientation defined as β; joint connectivity rate defined as k): (a) $\beta = 30^\circ$, $k = 0.3$; (b) $\beta = 30^\circ$, $k = 0.45$; (c) $\beta = 30^\circ$, $k = 0.6$; (d) $\beta = 45^\circ$, $k = 0.3$; (e) $\beta = 45^\circ$, $k = 0.45$; (f) $\beta = 45^\circ$, $k = 0.6$; (g) $\beta = 60^\circ$, $k = 0.3$; (h) $\beta = 60^\circ$, $k = 0.45$; (i) $\beta = 60^\circ$, $k = 0.6$.

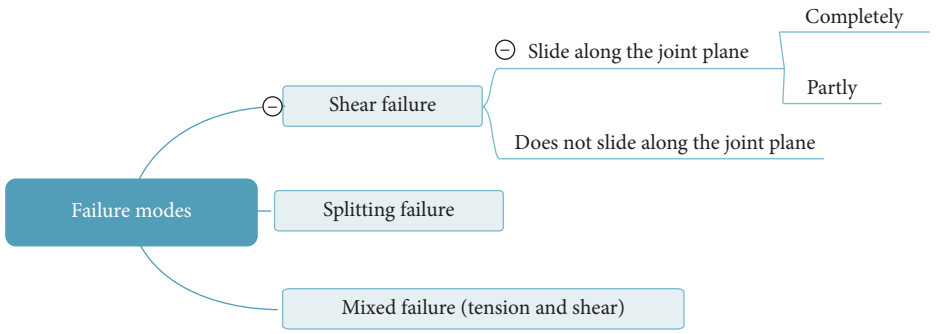

Figure 6: Failure modes.

(a)

(b)

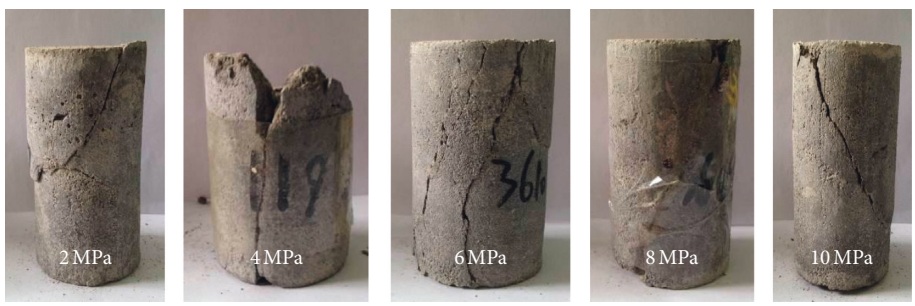

(c)

(d)

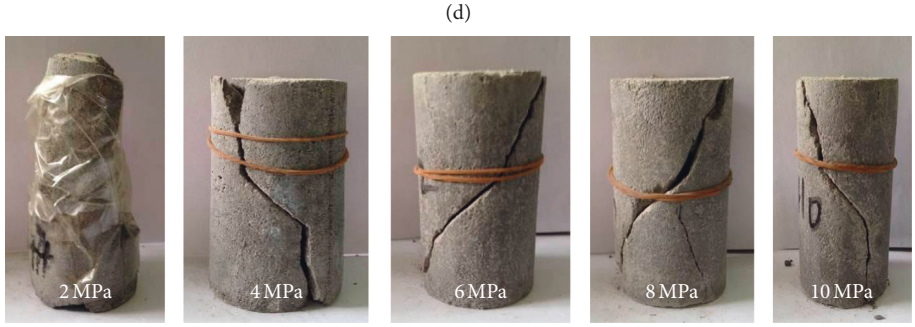

(e)

Figure 7: Continued.

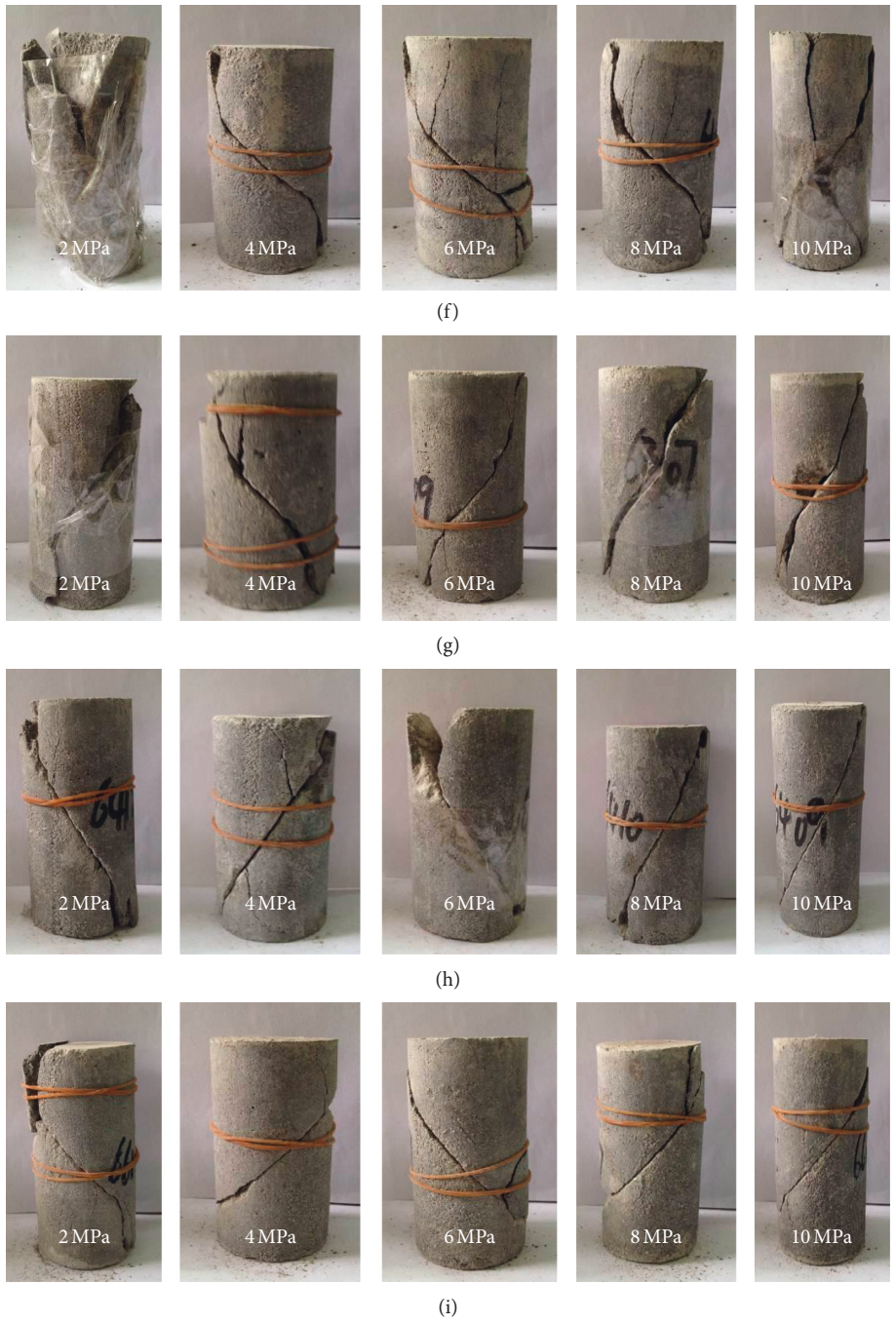

Figure 7: Sample failures under different pressures (joint orientation defined as β; joint connectivity rate defined as k): (a) $\beta = 30^\circ$, $k = 0.3$; (b) $\beta = 30^\circ$, $k = 0.45$; (c) $\beta = 30^\circ$, $k = 0.6$; (d) $\beta = 45^\circ$, $k = 0.3$; (e) $\beta = 45^\circ$, $k = 0.45$; (f) $\beta = 45^\circ$, $k = 0.6$; (g) $\beta = 60^\circ$, $k = 0.3$; (h) $\beta = 60^\circ$, $k = 0.45$; (i) $\beta = 60^\circ$, $k = 0.6$.

cannot be reconstructed to form intact specimens (Figure 7(d)). The amount of cracks initiated during the test was also considered as a parameter to characterize the effect of confining pressures. Note that the amount of crack is inversely proportional to the confining pressure. Here, the confining pressure was designated by σ_3. The fracture exhibited a continuous line-type crack at higher confining pressures (i.e., 8 and 10 megapascals). However, the crack showed a fork-like pattern when the confining pressure was less than 4 MPa. At lower confining pressures, samples were more vulnerable for damages during the unloading test. The phenomena were explained in terms of the restraint effect of confining pressure on the lateral deformation of the specimens. According to Mohr–Coulomb failure criterion, the deviatoric stress ($\sigma_1 - \sigma_3$) will increase when the confining pressure (σ_3) decreases, and the failure envelop can be easily reached. Meanwhile, internal defects were rapidly propagating as the deviatoric stress increased. Lastly, perforated

cracks emerged. On the contrary, internal defects were squeezed by the confining pressure. Hence, higher values of confining pressures can impose a significant restraint against the lateral deformations. Similarly, excavation can be regarded as unloading condition in rock slope engineering.

6.2. Effect of Orientation on the Failure Modes. In nature, rocks have different orientations of joints which affect their physical and mechanical properties. In this study, the relationships between joint orientations and crack propagations were studied. Obviously, the failure modes for different joint orientations were divergent. As shown in Figure 6, splitting failure was the predominant failure type for specimens with 30° joint orientations (Figures 7(a)–7(c)). Hence, joints with mild slopes have relatively small impact on the properties of rocks. On the contrary, mixed types of failures have been noticed on the specimens with 45° joints. During testing, the specimens were fragmented into pieces. In fact, it was difficult to trace the failure paths. However, at 60° joint orientation, shear failure was the predominant one. A flat surface was formed as a result of flaw cuttings. Hence, at 60° joint orientation, dislocations of pieces occurred due to a noticeable sliding.

6.3. Effect of Joint Connectivity Rate on the Failure Modes. For different joint angles, the effect of connectivity rate (k) is distinct. It had a considerable effect when the joint angles were 45° or 60°. However, at 30° joint angle, the effect of joint connectivity was relatively small. The path of crack propagation was twisted when the value of k was 0.3 (Figures 7(a), 7(d), and 7(g)). This is because of the restraint action of uncracked section of the specimens against sliding. The rupture face was rough since it is a result of multiple factors. On the one hand, joint and rock bridge alter or replace each other in accordance with the connectivity rate. On the other hand, the nonlinear variation of tension stress at the tip of flaws exists. As is shown in Figure 6, the crack path was becoming edge shaped when the value of k increased. Meanwhile, the failure modes gradually changed by the joints. Higher values of k yielded the straight plane of ruptures. Nonetheless, the concentrations of stresses were noticeable as shown in the development of secondary cracks (Figures 7(e) and 7(f)). The cracks were extended between the tips of the joints and the edges of the specimens when the joint angle and the connectivity rate were 45° and 0.45, respectively. For small values of k, the crack pattern became polygonal. However, the crack pattern was transforming into an arc shape when the value of k increased. Besides, the secondary cracks became normal to the edge of the specimens during shearing. At 60° joint orientation, there was no remarkable effect on the failure modes due to the variations of joint connectivity rate (k). All surfaces of failures were nearly flat. Nonetheless, there was a slight discrepancy between them. Similar failure modes were developed, when joint orientation and connectivity rate were 45° and 0.3, respectively. The significant effect of joint connectivity rate was obvious. Hence, shear failures can easily develop, and their probability of occurrence depends on the values of k. Shear failures were developed at higher values of k (Figures 7(h) and 7(i)).

Table 3 summarizes different types of failure modes for specimens with diverse joint orientations and connectivity rates. The failure mode was governed by the joint parameters. Fundamentally, the failure modes depend on the joint orientations initially. For instance, splitting failure is unlikely to occur when the joint angle is above 45°. Meanwhile, connectivity rate determines the extent of shear failure. The k values control the transformation between mixed and complete shear failures. At 60° joint orientation, both types of failures were observed. The critical value for k was 0.3 in this case.

7. Discussions of Crack Force Analysis Based on Griffith's Theory

Mohr–Coulomb and Griffith criteria are conventionally used to interpret the failure of rock specimens. It is noticeable that the Mohr–Coulomb criterion cannot clarify the influence of inside flaws on rock sample failure. However, maximum tensile stress in the perimeter of Griffith's crack (Figure 8) can be analyzed according to Griffith's theory for the sake of exploring the effectiveness of the internal defects.

Han et al. [26] deduced equation (2), a function of α and γ, considering primary stress of equation (1) and Inglis's formula:

$$\begin{cases} \sigma_y = \dfrac{\sigma_1 + \sigma_3}{2} + \dfrac{\sigma_1 - \sigma_3}{2}\cos 2\gamma, \\ \sigma_x = \dfrac{\sigma_1 + \sigma_3}{2} - \dfrac{\sigma_1 - \sigma_3}{2}\cos 2\gamma, \\ \tau_{xy} = -\dfrac{\sigma_1 - \sigma_3}{2}\sin 2\gamma, \end{cases} \tag{1}$$

$$\sigma_b = \frac{\sigma_1}{m^2 + \alpha^2}\left\{m\left(1 + \alpha^2\right)(1 + \lambda) + (1 + m)\left(m - \alpha^2\right)(1 - \alpha)\cos 2\gamma + \alpha(1 + m)^2(1 - \lambda)\sin 2\gamma\right\}. \tag{2}$$

Table 3: Failure modes for different types of samples.

	Connectivity rate		
Orientation	0.3	0.45	0.6
30	Splitting	Splitting	Splitting
45	Mixed	Mixed	Mixed
60	Mixed	Shear	Shear

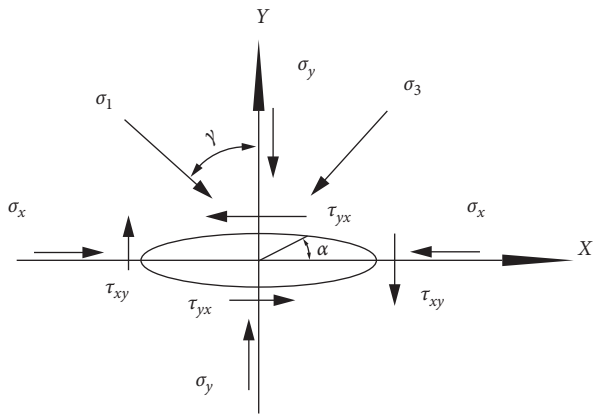

Figure 8: Stress state of the crack based on Griffith's theory [26].

As shown in the specimen schematic diagram, α and the crack width can be valued as 0°and 1 mm, respectively, since the crack is long and thin. Hence, the following equation is attained from equation (2):

$$\sigma_b = \frac{\sigma_1}{m}\{(1+\lambda)+(1+m)(1-\lambda)\cos 2\gamma\}. \quad (3)$$

The stress extremum hinges on σ_1, λ, and m at the tips of the crack in the condition of $\gamma = -(\pi/2)$. The equation is obtained as follows:

$$\sigma_0 = \frac{\sigma_1}{m}\{2\lambda - m(1-\lambda)\}. \quad (4)$$

According to equation (4), the maximum tensile stress at the tips of flaw was calculated. Meanwhile, the influences on the maximum tensile stress were analyzed considering joint inclined angles, joint connectivity, and confining pressures (Figures 9 and 10). Obviously, the maximum tensile stress increases promptly in accordance with the confining pressures. Simultaneously, higher joint connectivity rates lead to a large stress extremum. And the confining pressure enlarges this trend. As it is shown in Figure 10, the escalation of joint orientation boosts the maximum tensile stress at the tips of flaw. Therefore, the alteration of confining pressure is of most significant on the variation of the tensile stress, while the joint angle contributes the minimal impact.

With confining pressure (i.e., λ) declining gradually in the unloading stage, the longitudinal crack may arise due to extremum of tensile stress on the tips, and when it satisfies the fracture strength, the rupture of the longitudinal crack appears along the plane of the crack and may propagate continuously to the specimen's failure. Considering the axial stress stops expansion in the unloading stage, the specimen cannot be broken by some slanting cracks or crossed cracks

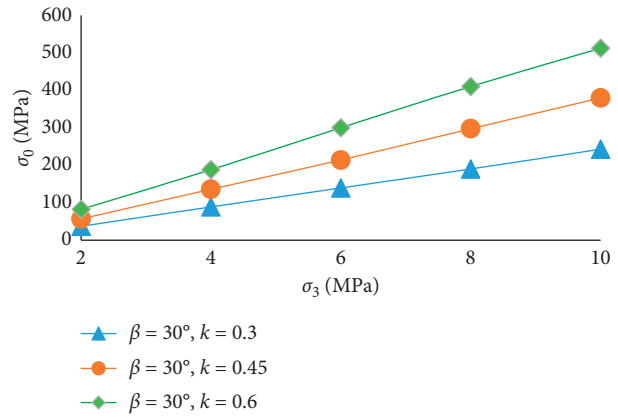

Figure 9: The stress extremum with 30° joint angle under different confining pressures.

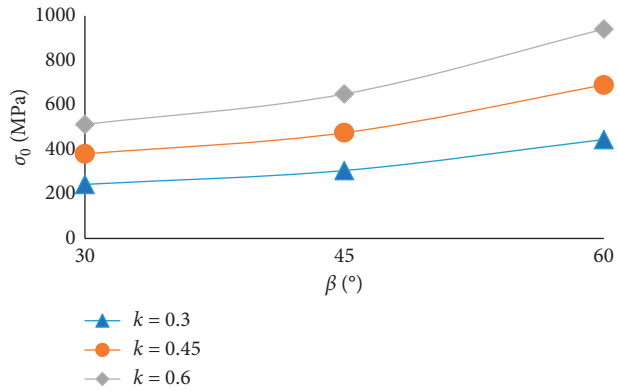

Figure 10: The stress extremum under different joint orientations and connectivity rates.

directly during the compression. Therefore, the splitting failure coupled with shear failure emerges finally.

8. Conclusions

In the preceding pages, the crack propagation was studied on the specimens with partially cut-through joints. The prime objective of this study was to examine the effect of joint orientations and joint connectivity rates on the mechanical characteristics of specimens. Even though nonlinear mechanical characteristics were observed, the macroscopic behavior was studied based upon the different values of joint geometries. Furthermore, nine types of specimens were used to investigate the failure mechanisms at different confining pressures. The confining pressure, joint orientation, and connectivity rate were considered as key parameters to analyze different failure modes. Finally, Griffith's theory was used to analyze the maximum tensile stress. Nevertheless, a further study is important to extend the application of this study in real engineering problems. The main findings of this paper are summarized below.

A nonlinear correlation was observed among the elasticity modulus, joint orientation, and joint connectivity rate. Meanwhile, the confining pressure was arithmetically

increasing. During the unloading stage, the reduction of deformation modulus can be used to predict the rock specimen failure. And the critical value of decrease percentage is 80%. The deformation modulus is less sensitive to the change of joint connectivity, whereas it is more sensitive to the change of the inclination angle.

Three different types (shear, split, and mixed) of failure modes were observed. The higher values of confining pressure can restraint the lateral deformation. At 30° joint orientation, the predominant failure was splitting failure. Similarly, mixed failures were observed at 45° joint orientations because of the concentration of stresses at the tip of the joints. On the contrary, shear failure was quite common due to sufficient length of 60° joint orientation. Comparatively, the effect of joint connectivity rate was smaller than that of the joint orientation. However, there was a clear variation in the crack propagation when the joint angle was 60°. The position of joints plays a significant role for anisotropic failures.

A few equations were introduced based on Griffith's theory to evaluate the maximum tensile stress at the tips of the crack. The results based on the calculation reveal the impaction of joint characteristics on the stress extremum.

Abbreviations

γ: The angle of principal stress σ_1 and Y axis
α: The central angle of the ellipse
m: The ratio of the minor axis (b) to major axis (a) of the ellipse
λ: The ratio of two principal stresses between σ_3 and σ_1
σ_0: The maximum tensile stress
σ_1: The maximum principal stress
σ_3: The minimum principal stress
σ_b: Tangential stress on the perimeter of a slender ellipse.

Data Availability

The data used to support the findings of this study may be released upon application to the China Three Gorges University Review Board, which can be done by contacting the author "Guoyong Duan (dgy@hhu.edu.cn)".

Conflicts of Interest

The authors wish to confirm that there are no known conflicts of interest associated with this publication and there has been no significant financial support for this work that could have influenced its outcome. Accordingly, the alteration of confining pressure is of most significance on the variation of the tensile stress, while the joint angle contributes the minimal impact.

Acknowledgments

The authors gratefully acknowledge the financial support from the National Natural Science Foundation of China (Grant nos. 51439003 and 51279091), the Fundamental Research Funds for the Central Universities (Hohai University) (Grant no. 2016B43014), Open Fund of Key Laboratory of Geological Hazards on Three Gorges Reservoir Area (China Three Gorges University) (Grant no. 2015KDZ12), and Key Project of Scientific Research Plan of Hubei Provincial Department of Education (Grant no. D20181202).

References

[1] T. Liu, P. Cao, and H. Lin, "Evolution procedure of multiple rock cracks under seepage pressure," *Mathematical Problems in Engineering*, vol. 2013, Article ID 738013, 11 pages, 2013.
[2] E. Hoek, "Strength of jointed rock masses," *Geotechnique*, vol. 33, no. 3, pp. 187–223, 1983.
[3] E. Hoek and Z. T. Bieniawski, "Brittle fracture propagation in rock under compression," *International Journal of Fracture*, vol. 26, no. 4, pp. 276–294, 1984.
[4] M. Basista and D. Gross, "The sliding crack model of brittle deformation: an internal variable approach," *International Journal of Solids and Structures*, vol. 35, no. 5-6, pp. 487–509, 1998.
[5] I. Vardoulakis, J. F. Labuz, E. Papamichos, and J. Tronvoll, "Continuum fracture mechanics of uniaxial compression on brittle materials," *International Journal of Solids and Structures*, vol. 35, no. 31-32, pp. 4313–4335, 1998.
[6] A. Paluszny and S. K. Matthäi, "Numerical modeling of discrete multi-crack growth applied to pattern formation in geological brittle media," *International Journal of Solids and Structures*, vol. 46, no. 18-19, pp. 3383–3397, 2009.
[7] R.-H. Cao, P. Cao, H. Lin, C.-Z. Pu, and K. Ou, "Mechanical behavior of brittle rock-like specimens with pre-existing fissures under uniaxial loading: experimental studies and particle mechanics approach," *Rock Mechanics and Rock Engineering*, vol. 49, no. 3, pp. 763–783, 2016.
[8] X. Fan, R. Chen, H. Lin, H. Lai, C. Zhang, and Q. Zhao, "Cracking and failure in rock specimen containing combined flaw and hole under uniaxial compression," *Advances in Civil Engineering*, vol. 2018, Article ID 9818250, 15 pages, 2018.
[9] D. Bing, H. Guicheng, and Z. Zhijun, "A numerical research on crack process of gypsum containing single flaw with different angle and length in uniaxial loading," *Shock and Vibration*, vol. 2018, Article ID 2968205, 16 pages, 2018.
[10] J. Zhang, "Investigation of relation between fracture scale and acoustic emission time-frequency parameters in rocks," *Shock and Vibration*, vol. 2018, Article ID 3057628, 14 pages, 2018.
[11] X. Meng and W. Liu, "Study on failure process and permeation evolution of single-cracked rock," *Advances in Materials Science and Engineering*, vol. 2018, Article ID 7915652, 9 pages, 2018.
[12] M. Sagong, D. Park, J. Yoo, and J. S. Lee, "Experimental and numerical analyses of an opening in a jointed rock mass under biaxial compression," *International Journal of Rock Mechanics and Mining Sciences*, vol. 48, no. 7, pp. 1055–1067, 2011.
[13] W. Chen, H. Konietzky, X. Tan, and T. Frühwirt, "Pre-failure damage analysis for brittle rocks under triaxial compression," *Computers and Geotechnics*, vol. 74, pp. 45–55, 2016.
[14] S.-Q. Yang, P. G. Ranjith, Y.-H. Huang et al., "Experimental investigation on mechanical damage characteristics of sandstone under triaxial cyclic loading," *Geophysical Journal International*, vol. 201, no. 2, pp. 662–682, 2015.
[15] N. Erarslan, "Microstructural investigation of subcritical crack propagation and fracture process zone (FPZ) by the

reduction of rock fracture toughness under cyclic loading," *Engineering Geology*, vol. 208, pp. 181–190, 2016.

[16] X. Wang, Y. Jiang, and B. Li, "Experimental and numerical study on crack propagation and deformation around underground opening in jointed rock masses," *Geosciences Journal*, vol. 21, no. 2, pp. 291–304, 2017.

[17] X. P. Zhou and H. Yang, "Damage by cracking of rock mass induced by dynamic unloading in the high slopes of the three gorges project permanent shiplock," *International Journal of Terraspace Science & Engineering*, vol. 1, no. 1, pp. 47–58, 2009.

[18] J.-H. Hu, T. Lei, K.-P. Zhou, X.-W. Luo, and N.-G. Yang, "Mechanical response of roof rock mass unloading during continuous mining process in underground mine," *Transactions of Nonferrous Metals Society of China*, vol. 21, no. 12, pp. 2727–2733, 2011.

[19] S. Zhou, X. Zhuang, H. Zhu, and T. Rabczuk, "Phase field modelling of crack propagation, branching and coalescence in rocks," *Theoretical and Applied Fracture Mechanics*, vol. 96, pp. 174–192, 2018.

[20] X. Z. Li, Z. S. Shao, and L. F. Fan, "A micro-macro method for predicting the shear strength of brittle rock under compressive loading," *Mechanics Research Communications*, vol. 75, pp. 13–19, 2016.

[21] J. Xu, J. Jiang, L. Zuo, and Y. Gao, "Acoustic emission monitoring and failure precursors of sandstone samples under various loading and unloading paths," *Shock and Vibration*, vol. 2017, Article ID 9760940, 11 pages, 2017.

[22] Q. Tan, R. Zhang, M. Gao, Q. Liu, Z. Zhang, and Z. Jia, "Coal permeability and crack distribution characteristics in unloading confining pressure experiments under different water pressures," *Thermal Science*, vol. 21, no. 1, pp. 241–249, 2017.

[23] H. Yang, J. Liu, and X. Zhou, "Effects of the loading and unloading conditions on the stress relaxation behavior of precracked granite," *Rock Mechanics and Rock Engineering*, vol. 50, no. 5, pp. 1157–1169, 2017.

[24] D. Li, Z. Sun, T. Xie, X. Li, and P. G. Ranjith, "Energy evolution characteristics of hard rock during triaxial failure with different loading and unloading paths," *Engineering Geology*, vol. 228, pp. 270–281, 2017.

[25] H. Liu and L. Zhang, "A damage constitutive model for rock mass with nonpersistently closed joints under uniaxial compression," *Arabian Journal for Science and Engineering*, vol. 40, no. 11, pp. 3107–3117, 2015.

[26] L. Han, Y. He, and H. Zhang, "Study of rock splitting failure based on griffith strength theory," *International Journal of Rock Mechanics and Mining Sciences*, vol. 83, pp. 116–121, 2016.